Published in final edited form as:
Development. 2008 November ; 135(22): 3775–3787. doi:10.1242/dev.021238.

Restriction of retinoic acid activity by Cyp26b1 is required for proper timing and patterning of osteogenesis during zebrafish development

Kathrin Laue[1,2], **Martina Jänicke**[1,2], **Nikki Plaster**[1,*], **Carmen Sonntag**[1], and **Matthias Hammerschmidt**[1,2,†]

[1]Max-Planck-Institute of Immunobiology, Stuebeweg 51, D-79108 Freiburg, Germany

[2]Institute for Developmental Biology, University of Cologne, D-50923 Cologne, Germany

Abstract

Skeletal syndromes are among the most common birth defects. Vertebrate skeletogenesis involves two major cell types: cartilage-forming chondrocytes and bone-forming osteoblasts. In vitro, both are under the control of retinoic acid (RA), but its exact in vivo effects remained elusive. Here, based on the positional cloning of the *dolphin* mutation, we have studied the role of the RA-oxidizing enzyme Cyp26b1 during cartilage and bone development in zebrafish. *cyp26b1* is expressed in condensing chondrocytes as well as in osteoblasts and their precursors. *cyp26b1* mutants and RA-treated wild-type fish display a reduction in midline cartilage and the hyperossification of facial and axial bones, leading to fusions of vertebral primordia, a defect not previously described in the context of RA signaling. Fusions of cervical vertebrae were also obtained by treating mouse fetuses with the specific Cyp26 inhibitor R115866. Together with data on the expression of osteoblast markers, our results indicate that temporal and spatial restriction of RA signaling by Cyp26 enzymes is required to attenuate osteoblast maturation and/or activity in vivo. *cyp26b1* mutants may serve as a model to study the etiology of human vertebral disorders such as Klippel-Feil anomaly.

Keywords

Cyp26b1; Retinoic acid; Bmp2; Cartilage; Bone; Chondrocyte; Osteoblast; Osteopontin; Osterix; Craniofacial development; Vertebra; Zebrafish

INTRODUCTION

Skeletal development is highly conserved in vertebrates and involves two main processes: skeletal patterning to define the shape and location of the different skeletal elements within the developing body, and differentiation of skeletogenic cells (Karsenty and Wagner, 2002; Mariani and Martin, 2003). Cartilage-forming chondrocytes and bone-forming osteoblasts share a common mesenchymal progenitor that derives from neural crest, sclerotome or lateral plate mesoderm (Olsen et al., 2000). Skeletogenesis is initiated when mesenchymal cells aggregate to form mesenchymal condensations. In most parts of the bony skeleton, including the vertebral column of mammals, but not of teleosts (Bird and Mabee, 2003;

†Author for correspondence (mhammers@uni-koeln.de).
*Present address: Department of Developmental and Cell Biology, UCI, Irvine, CA 92697, USA

Supplementary material
Supplementary material for this article is available at http://dev.biologists.org/cgi/content/full/135/22/3775/DC1

Elizondo et al., 2005; Fleming et al., 2004; Inohaya et al., 2007), a cartilaginous anlage serves as a template to model the future bone (endochondral ossification). In this case, cells within the condensation become chondrocytes, whereas cells at the periphery of the skeletal element form a structure called the perichondrium (Karsenty and Wagner, 2002). During ossification, chondrocytes in the core of the condensate become hypertrophic, a transition reflected in the switch from *Col2a1* (encoding collagen type II) to *Col10a1* (collagen type X) expression, while osteoblasts start to mature within the perichondrium (now also called the periosteum) and form ossification centers that eventually replace the cartilage (Colnot, 2005; Karsenty and Wagner, 2002). Alternatively, some skeletal elements, including parts of the craniofacial system, are generated by direct differentiation of mesenchymal cells into osteoblasts (intramembranous or dermal ossification). Maturing osteoblasts express the same marker genes as hypertrophic chondrocytes, including the transcription factor gene *runx2* (also called *cbfa1*) (Flores et al., 2006; Flores et al., 2004), *osteopontin* (*opn*; also called *spp1*) (Kawasaki et al., 2004), which encodes a component of bone matrix (Alford and Hankenson, 2006), and, at least in zebrafish, *col10a1* (Avaron et al., 2006), whereas the transcription factor Osterix (Osx; also called Sp7) is a specific marker and regulator of the osteoblast lineage (Nakashima et al., 2002).

A known signal regulating skeletogenic cell development is all-trans retinoic acid (RA) (Adams et al., 2007; Weston et al., 2003), a derivative of vitamin A that is required for multiple processes of vertebrate development (Niederreither and Dolle, 2008). RA is a diffusible lipophilic molecule that binds to nuclear receptors [retinoic acid receptors (RARs) and retinoid X receptors (RXRs)] to regulate the transcription of target genes. RA concentrations are determined by the balance between RA synthesis via retinaldehyde hydrogenases (Aldh1-3) and RA oxidation by cytochrome P450 enzymes of the Cyp26 class (Blomhoff and Blomhoff, 2006; Fujii et al., 1997; White et al., 1997). As in mammals, three different zebrafish *cyp26* genes have been described: *cyp26a1*, *cyp26b1* and *cyp26c1* (formerly *cyp26d1*), which are expressed in distinct, but partially overlapping patterns (Abu-Abed et al., 2002; Emoto et al., 2005; Gu et al., 2005; Hernandez et al., 2007; Kudoh et al., 2002; MacLean et al., 2001; Tahayato et al., 2003; Zhao et al., 2005). The in vivo requirement for Cyp26 enzymes was revealed via *Cyp26a1* and *Cyp26b1* gene targeting in mouse (Abu-Abed et al., 2001; MacLean et al., 2007; Yashiro et al., 2004), and via *cyp26a1* (*giraffe*) mutants (Emoto et al., 2005) and antisense-mediated knockdown of *cyp26a1*, *cyp26b1* and *cyp26c1* in zebrafish (Echeverri and Oates, 2007; Hernandez et al., 2007; Kudoh et al., 2002; Reijntjes et al., 2007; Shelton et al., 2006; White et al., 2007). Of the zebrafish reports, only one addressed the role of Cyp26 enzymes during skeletogenesis, claiming that Cyp26b1 is required for the patterning and migration of cranial neural crest (Reijntjes et al., 2007).

Knockout of *Cyp26b1* in mouse causes severe limb defects that have been attributed to a combination of shifts in the proximodistal patterning of the limb bud and a retardation of chondrocyte maturation (Yashiro et al., 2004). This suggests that Cyp26b1 interferes with the reported role of RA in blocking chondrocyte specification from mesenchymal precursors (Weston et al., 2003). Other data suggest a later and seemingly opposing role for RA signaling in promoting hypertrophic maturation of chondrocytes and subsequent replacement by bone (Weston et al., 2003), although this has not yet been addressed genetically. Also, it has remained unclear to what extent this latter effect is due to interference with chondrocytes (Iwamoto et al., 1993; Weston et al., 2003) versus osteoblasts (Manji et al., 1998; Song et al., 2005) and with osteoblast maturation versus activity.

Here, we have studied the role of Cyp26b1 as an essential regulator of skeletal development in zebrafish. *cyp26b1* is expressed in chondrogenic mesenchymal condensations as well as

in osteoblast precursors of endochondral and intramembranous bones, including vertebrae. *cyp26b1* mutants display multiple defects during chondro- and osteogenesis, all of which can be mimicked by treatment with RA. This indicates that in contrast to a recent report (Reijntjes et al., 2007), zebrafish Cyp26b1 acts by restricting retinoid signaling. The hyperossification of craniofacial bones and vertebrae of mutant animals is anticipated by an increase in *osteopontin* expression in osteoblasts. Comparing the axial defects of *cyp26b1* mutants with those caused by transgenic overexpression of the Bone morphogenetic protein Bmp2, a well-known positive regulator of osteoblast maturation upstream of Runx2 and Osx (Ulsamer et al., 2008; Wu et al., 2007), we noticed striking differences in the pattern of hyperossification and in the molecular signature of the supernumerary osteoblasts. Together, these data suggest that RA inhibition by Cyp26 enzymes is required to restrict ossification in vivo, most likely by attenuating osteoblast activity.

MATERIALS AND METHODS

Zebrafish lines

Unless noted otherwise, the *dol* allele *ti230g* was used (Piotrowski et al., 1996). For temporally controlled *bmp2b* overexpression, the transgenic line *Tg(hsp70:bmp2b)* was used as described (Chocron et al., 2007). According to RT-PCR analyses, the transgene is activated within 10 minutes after the heat shock, with transcripts remaining detectable for ~24 hours.

Mapping and cloning of *dol*/*cyp26b1*

Genetic rough mapping of dol^{ti230g} was carried out via bulk meiotic segregation analyses as described (Laue et al., 2008). For chromosomal walking, the BAC libraries CHORI-211 and DanioKey (RZPD) were screened by PCR. For identification of the mutant lesion and for genotyping, genomic *cyp26b1* DNA or cDNA (GenBank accession number AY321366) fragments were amplified by PCR and sequenced. Primer sequences are available upon request.

Morpholino oligonucleotide (MO) injections

An MO against the *cyp26b1* splice-donor junction between exon 3 and intron 3 (Cyp26b1-SDEx3 MO, 5′-AGCTATTGACATTTTAC-CTTTCTGT-3′) was purchased from Gene Tools. For full knockdown, ~0.5 pmol, and for hypomorphs (Fig. 6E), 0.2 pmol, of MO was injected per embryo at the one-cell stage as described (Nasevicius and Ekker, 2000). *aldh1a* MO was used as described (Begemann et al., 2001).

Tissue labeling procedures

In situ hybridization and fluorescent double in situ hybridization were performed as described (Clay and Ramakrishnan, 2005; Hammerschmidt et al., 1996). For zebrafish *opn* and *osx*, cDNA fragments were amplified by RT-PCR with primer sequences obtained from the Ensembl database, and cloned into pCRII-TOPO (Invitrogen). For probe synthesis, plasmids were linearized with *Xho*I and transcribed with SP6 RNA polymerase. For *cyp26b1*, clone IMAGp998A0411194Q1 was obtained from RZPD, linearized with *Kpn*I and transcribed with SP6 RNA polymerase. Probes for *cyp26a1* and *cyp26c1* (Hernandez et al., 2007), *col2a1* (Yan et al., 1995), *col10a1* (Nica et al., 2006), *dlx2a* (Akimenko et al., 1994) and *sox9a* (Wada et al., 2005) were synthesized as described.

Immunostainings were carried out using the Vectastain ABC Kit (Axxora) with the following primary antibodies and dilutions: zn5 (1:500, ZIRC, University of Oregon), anti-GFP (1:200, Roche). For sectioning, embryos were embedded in paraffin.

Skeletal elements of zebrafish and mice were stained with Alcian Blue and/or Alizarin Red essentially as described (Kessel and Gruss, 1991; Walker and Kimmel, 2007).

Drug treatments

Stock solutions (10 mM) of 4-(diethylamino)benzaldehyde (DEAB; Fluka), all-trans RA (Sigma) and R115866 (Johnson and Johnson Pharmaceutical Research and Development) were prepared in DMSO as described (Begemann et al., 2004; Begemann et al., 2001; Hernandez et al., 2007). Wild-type or *cyp26b1* mutant zebrafish were incubated in the dark with final concentrations of 0.5 μM RA (before 50 hpf), 10 μM RA (after 48 hpf), 10 μM DEAB (before 50 hpf), 50 μM DEAB (after 48 hpf) or 10 μM R115866. For mouse experiments, R115866 was dissolved in PEG 200 (Sigma, 2.5 mg/ml) and administered to pregnant NMRI females by daily oral gavages, applying 10 mg per kilogram body weight, from E13–16.

RESULTS

The phenotype of *dolphin* mutants is caused by Cyp26b1 loss-of-function

The *dolphin* mutant *dol*^{ti230g}, which was previously identified in a large-scale ENU mutagenesis screen, is characterized by a beak-like appearance of the jaw (Fig. 1A, B) (Piotrowski et al., 1996) and, in some genetic backgrounds, by shorter and malformed pectoral fins (Fig. 1C, D). Using bulk segregation linkage analysis, the *dolphin* locus was mapped to a 0.38 cM interval on linkage group 7 (Fig. 1E); this was followed by a BAC walk to construct a contig covering the interval (Fig. 1F). Newly designed markers (KL1-7) along three overlapping BACs within the contig showed no recombination in 4500 meioses (Fig. 1F).

The three BACs contained several genes, all of which were sequenced. Only in the *cyp26b1* gene of mutants was a mutation found, comprising a GT→AT transition in the splice-donor site of the exon 3-intron 3 junction (Fig. 1H, I). Sequencing of independent cDNA clones revealed the use of a downstream GT as a novel splice-donor in mutants (50/50), but not in wild-type embryos of the same strain (0/50) (Fig. 1I, J). The resulting transcript carries an insertion of seven nucleotides, leading to a frame shift and premature termination of the protein. This C-terminal truncation removes most of the highly conserved cytochrome P450 domain, including the oxygen-, steroid- and heme-binding sites (Fig. 1G). Subsequently, a second *cyp26b1* allele, *sa0002*, was identified by TILLING (Wienholds et al., 2003), with an AAG→TAG nonsense mutation at nucleotide position 135 of the coding region, causing an even more severe truncation of the protein after 45 amino acid residues (Fig. 1G) (http://www.sanger.ac.uk/cgi-bin/Projects/D_rerio/mutres/tracking.pl). *sa0002* failed to complement *ti230g*, and *sa0002* mutants showed craniofacial and axial defects indistinguishable from those of *ti230g* mutants (see Fig. S1A–C, E–G in the supplementary material). In contrast to full-length Cyp26b1, both truncated versions were completely inactive upon forced expression in early zebrafish embryos (see Fig. S1I–L in the supplementary material). Furthermore, the axial hyperossification of *ti230g* mutants could be rescued or converted to hypo-ossified phenotypes by temporally controlled reapplication of wild-type *cyp26b1* (see Fig. S1H in the supplementary material). Finally, the defects of *dol* mutants could be phenocopied in wild-type fish by injecting an antisense MO targeting the splice site affected in the *ti230g* allele (Fig. 4G, N; Fig. 5C; Fig. 6E, F; see Fig. S2 in the supplementary material). Together, this indicates that the defects of zebrafish *dol* mutants are caused by null mutations in the *cyp26b1* gene.

cyp26b1 is expressed in cranial precartilage condensations, perichondrial cells and osteoblasts

cyp26b1 has been shown to be expressed in various regions of zebrafish embryos (Hernandez et al., 2007; Zhao et al., 2005). We have extended these studies, focusing on developing skeletal elements. At 26 hours post-fertilization (hpf), *cyp26b1* was expressed in multiple domains in close proximity to postmigratory cranial neural crest (CNC) cells, but not in CNC itself, as revealed by double stainings with *cyp26b1* and the CNC markers *dlx2a* or *fli1a* (Fig. 2A–D). *cyp26b1* was prominently expressed in the forehead close to the CNC that, according to cell-tracing experiments, gives rise to chondrocytes of the neurocranial ethmoid plate (Eberhart et al., 2006; Wada et al., 2005) (Fig. 2A, B). In addition, *cyp26b1* was expressed adjacent to postmigratory CNC that gives rise to the pharyngeal arches (Fig. 2C, D).

At 48 hpf, *cyp26b1* was coexpressed with *sox9a* (Fig. 2H) in mesenchymal condensations that give rise to pharyngeal arches (Fig. 2F) and neurocranial cartilages (Fig. 2G). However, concomitant with the onset of *col2a1* expression, which is a marker for specified chondrocytes (Yan et al., 1995), *cyp26b1* expression ceased within the cartilaginous elements but remained strong in perichondrial cells (Fig. 2I–K). A similar transient expression in mesenchymal condensations and persistent expression in perichondria of the craniofacial skeletal elements has also been described for mouse *Cyp26b1* (Abu-Abed et al., 2002). The perichondrium is a supposed source of osteoblasts. However, in contrast to widespread perichondrial expression of *cyp26b1*, expression of the osteoblast markers *osterix* (*osx*) (Fig. 2L), *osteopontin* (*opn*) (Fig. 2M) and *col10a1* (Fig. 2N) (Avaron et al., 2006) was confined to those perichondrial domains undergoing endochondral ossification (Fig. 2O). In such *col10a1*-positive cells, *cyp26b1* transcript levels were lower than in the adjacent *col10a1*-negative perichondrium (Fig. 2P, Q), suggesting that *cyp26b1* expression decreases when osteoblasts differentiate and/or become active.

In addition to the perichondrium/periosteum, zebrafish *cyp26b1* was expressed in various bone primordia that ossify in an intramembranous manner (Cubbage and Mabee, 1996; Elizondo et al., 2005). Examples include the opercle (Fig. 3A, D) and cleithrum (see Fig. S4G in the supplementary material). At 72 and 120 hpf, the opercular bone matrix (Fig. 3C, F) was surrounded by osteoblasts coexpressing *col10a1*, *osx* and *opn* (Fig. 3B, E; see S4A–F in the supplementary material). Double in situ hybridization for *cyp26b1* and *col10a1* further revealed that, similar to in the perichondrium, *cyp26b1* levels in *col10a1*-positive osteoblasts of the opercle (Fig. 3A, D) and cleithrum (see Fig. S4G in the supplementary material) were considerably weaker than in adjacent cells, which are most likely immature and/or less active osteoblasts.

Osteoblast expression of *cyp26b1* was also found in the elements of the axial skeleton. The anterior part of the notochord, which becomes uniformly ossified (basioccipital articulatory process) (see Fig. 6A), was lined by a continuous layer of *cyp26b1*-positive cells (Fig. 3G), whereas in trunk and tail, where ossification of vertebral primordia occurs in a segmented manner, *cyp26b1*-positive cells displayed a corresponding metameric distribution (Fig. 3H, I). The same metameric pattern was obtained for the osteoblast markers *opn* and *col10a1* (Fig. 3L–N). The position of such osteoblasts at intersomitic borders coincided with the anterior borders of forming vertebral bodies stained with Alizarin Red (Fig. 3O), suggesting that cells were localized within the intervertebral zones. Comparative expression analyses at different developmental time points further revealed a continuous decline in the number of axial *cyp26b1*-positive cells from 96–156 hpf, while the number of *col10a1*- and *opn*-positive cells increased (Fig. 3P), with transient coexpression of *cyp26b1* and *opn* in the same cells at 144 hpf (Fig. 3J).

cyp26b1 mutants lack cartilaginous elements in the midline of the neurocranium and pharyngeal arches

Alcian Blue stainings of the cartilage of *cyp26b1* mutants and morphants at 120 hpf revealed specific defects in midline elements of the visceral skeleton and the neurocranium, whereas most other cartilaginous elements appeared largely normal (Fig. 4E–G). The ceratohyals of the left and right second arches were fused in the midline (Fig. 4H, I), and the medial elements (basibranchial) of the posterior gill arches (p5, p6) were missing (Fig. 4J, K). In addition, the medial ethmoid plate of the neurocranium was missing or strongly reduced (Fig. 4L–N), very similar to the phenotype previously described for mutants in *sonic hedgehog* (Wada et al., 2005). To determine when this defect arises, we stained embryos for *col2a1*and *sox9a* to label chondrocytes and their precursors. At 36 hpf, *col2a1* is expressed in chondrocyte precursors of the trabeculae cranii (Fig. 4A), which are lateral structures of the neurocranium surrounding the ethomoid plate and extending further posteriorly (Schilling and Kimmel, 1997). At this stage, *col2a1* expression in *cyp26b1* mutants appeared normal (Fig. 4B). However, at 56 hpf, the *col2a1* expression domains were shifted posteriorly and fused at the midline, anticipating the subsequent absence of the medial ethmoid (Fig. 4C, D).

cyp26b1 mutants display hyperossification of craniofacial bones and axial skeleton, leading to the fusion of vertebral bodies

As in higher vertebrates, the majority of the zebrafish craniofacial skeleton forms through endochondral ossification, starting at 6 days post-fertilization (dpf); for example, in restricted regions of the ceratohyal and hyomandibula of the second pharyngeal arch. Intramembranous bones form even earlier, with mineralization of the opercle starting at 3 dpf (Cubbage and Mabee, 1996).

Staining *cyp26b1* mutants or morphants for mineralized bone matrix with Alizarin Red, we observed hyperossification of both endochondral and intramembranous bones. At 192 hpf, the mineralized domain in the opercle of mutants and morphants was larger than in wild-type animals (Fig. 5A–C). Also, mutants displayed significantly stronger and more advanced endochondral mineralization of the ceratohyal (Fig. 5D–F).

In addition to craniofacial defects, *cyp26b1* mutants and morphants exhibited severe abnormalities in the axial skeleton, which in teleost larvae is formed through ossification of the sheath around the notochord (perichordal ossification). In zebrafish, unsegmented ossification around the anterior part of the notochord gives rise to the basioccipital articulatory process, while metameric mineralization more posteriorly forms the vertebral column. Vertebral ossification starts at the level of the fourth vertebral body (centrum), from where it proceeds anteriorly and posteriorly (Bird and Mabee, 2003; Gavaia et al., 2006; Stemple, 2005). At 180 hpf, wild-type larvae exhibited six to eight Alizarin Red-positive centra, with centra 3 and 4 correspondingly broader than the others (Fig. 6A). By contrast, *cyp26b1* mutants and morphants showed a complete fusion of Alizarin Red-positive segments and an extension of staining into caudal regions, which in wild-type animals mineralize later (Du et al., 2001) (Fig. 6C, F). In cross-sections, the mineralized perichordal sheath of mutants appeared broader and more strongly stained than in wild-type siblings, whereas notochordal cells remained Alizarin Red-negative and normally vacuolated (Fig. 6G–J). Interestingly, *cyp26b1* heterozygotes and wild-type embryos injected with lower amounts of *cyp26b1* MO displayed an intermediate phenotype with distinct, but broader, centra in anterior regions and precocious centra mineralization in caudal regions of the notochord (Fig. 6, compare B, E with A, D). This suggests that Cyp26b1 is required to attenuate vertebral growth.

Treatment with RA phenocopies, and inhibition of RA synthesis rescues, the craniofacial and axial defects of *cyp26b1* mutants

In mouse, there is evidence for a negative effect of Cyp26 enzymes on retinoid signaling (Fujii et al., 1997; Niederreither et al., 2002; White et al., 1997). However, according to a recent study, the phenotype of the *cyp26b1* morphant zebrafish more closely resembles that of RA deficiency, suggesting that Cyp26 enzymes might generate, rather than metabolize, biologically active retinoids (Reijntjes et al., 2007). To test this, and to determine the crucial time window(s) of Cyp26b1 activity, we treated wild-type and *cyp26b1* mutant embryos for various time intervals with all-trans RA (RA excess) or the competitive Aldh inhibitor 4-(diethylamino)benzaldehyde (DEAB; RA deficiency).

Strikingly, RA treatment of wild-type embryos from 24 to 50 hpf caused the same neurocranial phenotype as in *cyp26b1* mutant embryos, characterized by the absence of the medial ethmoid plate at 120 hpf (Fig. 7A, B; compare with Fig. 4M) (n=25/25). By contrast, RA treatments commencing after 48 hpf did not alter anterior neurocranial morphology (data not shown). Conversely, DEAB treatment of *cyp26b1* mutants and morphants from 24 to 50 hpf rescued the ethmoid phenotype (Fig. 7D) (n=9/10), whereas the same treatment of wild-type embryos left neurocranial morphology intact (Fig. 7C) (n=29/29) but caused a reduction of gill arches, reminiscent of the phenotype of *aldh1a* mutants (Begemann et al., 2001). Together, this indicates that the anterior neurocranial cartilage defects of *cyp26b1* mutants are caused by RA excess during the second day of development.

Interference with bone development required significantly later treatments. Whereas RA treatment from 24 to 50 hpf had no effect on craniofacial ossification at 180 hpf (Fig. 7, compare F with E) (n=45/45), treatment from 72 to 96 hpf and onwards caused hyperossification of both endochondral and intramembranous bones (Fig. 7G) (n=25/26), comparable to that seen in *cyp26b1* mutants (Fig. 5B, E). Consistently, craniofacial ossification of mutants was significantly reduced upon DEAB treatment starting at 72 or 96 hpf (Fig. 7H). Similarly, treatment of wild-type larvae with RA or the specific Cyp26 inhibitor R115866 (Njar et al., 2006; Stoppie et al., 2000) from 96 hpf resulted in axial hyperossification at 180 hpf (Fig. 7K, L) (n=32/33 and 27/27), as in *cyp26b1* mutants (Fig. 7S), whereas earlier RA treatments (48–72 hpf) had no effect (Fig. 7J) (n=40/40). Conversely, ossification of centra was blocked or significantly reduced when wild-type or *cyp26b1* mutant larvae were treated with DEAB from 96 hpf (Fig. 7Q, R) (n=33/33). Intriguingly, a significant reduction in the axial hyperossification of *cyp26b1* mutants (Fig. 7M) to wild-type levels was obtained upon injection of *aldh1a* MO (Begemann et al., 2001) (Fig. 7S, T) (n=9/12). Together, this indicates that Cyp26b1 is required at different developmental stages to regulate skeletal patterning and ossification of skeletal elements by inactivating RA. This anti-RA effect is consistent with the data obtained in mouse, but in contrast to the conclusions by Reijntjes et al. described above (Reijntjes et al., 2007).

The temporal and spatial pattern of axial hyperossification caused by RA differs from that caused by Bmp2b

To gain insight into the cellular basis of RA-induced hyperossification, we compared the effects of RA application with those caused by excessive Bmp2, a well-known positive regulator of osteoblast maturation (Wu et al., 2007). For temporally controlled Bmp2 overexpression, we used transgenic fish that carry the *bmp2b* cDNA under the control of the heat-inducible *hsp70* promoter (Chocron et al., 2007). Applying the heat shock at 50 hpf, when RA applications had no effect on centra ossification (Fig. 7J), transgenic *bmp2b* fish displayed a fusion of centra 3-6 (Fig. 7O). These are the first ossifying centra during normal development (see above). By contrast, Bmp2 applied at 96 or 144 hpf left the early-ossifying centra unaffected, causing fusions of the later ossifying, more-anterior and more-posterior

vertebral bodies (Fig. 7P) (data not shown), whereas centra 3-6 were fused upon RA application at these later stages (Fig. 7K; see Fig. S6A, B in the supplementary material). Strikingly, fusions of centra 3-6 were even obtained upon RA administration at 12 or 15 dpf (Fig. 7M, N; see Fig. S6C–F in the supplementary material). This indicates that Bmp2 affects osteoblast precursors at stages when they are not yet sensitive to RA, whereas RA can still affect osteoblasts long after they have become insensitive to Bmp2.

cyp26b1 mutant osteoblasts display increased expression of *osteopontin*

To directly compare the effects of Cyp26b1/RA and Bmp2b on osteoblasts, we stained for the osteoblast markers *col10a1*, *osx*, *opn* and *cyp26b1* itself. In craniofacial skeletal elements of *cyp26b1* mutants, *cyp26b1* expression was much stronger than in wild-type siblings (Fig. 8A). Similarly, osteoblasts of the opercle of mutants displayed stronger *opn* expression. At 72 hpf, the number of *opn*-positive cells appeared normal, with higher expression levels per cell (Fig. 8B). However, at 120 hpf, there were supernumerary cells in normally *opn*-negative subdomains of the opercle (Fig. 8C). By contrast, expression levels and patterns of *osx* and *col10a1* appeared unaltered in mutants (Fig. 8D, E).

Similarly, in the axial skeleton, *cyp26b1* mutants displayed a striking increase in *cyp26b1*- and *opn*-positive cells, with premature expression and an extension into more-posterior trunk regions (Fig. 8F, G; see Fig. S7 in the supplementary material), whereas the number of *col10a1*-positive cells was normal (Fig. 8H). Ectopic *cyp26b1*-positive cells were present ventral of the notochord, in contrast to their preferential perichordal localization in wild-type siblings (Fig. 8F). According to previous studies, axial osteoblasts stem from the sclerotome in ventral-most regions of the somites, from where they move dorsally towards the notochord (Inohaya et al., 2007; Morin-Kensicki and Eisen, 1997), consistent with the ventral-to-dorsal progression of centra ossification (Fig. 6K). Thus, the ventral *cyp26b1*-positive cells are possibly immature osteoblasts that express *cyp26b1* precociously in the mutant.

By contrast, overexpression of Bmp2b left the number of *cyp26b1*-positive cells unaffected (Fig. 8I), suggesting that their increase in *cyp26b1* mutants might primarily reflect the loss of a negative RA→Cyp26 feedback loop, as described previously in other circumstances (Emoto et al., 2005). Strikingly, Bmp2b excess led to an increase not only of *opn*-positive, but also of *col10a1*-positive, cells (Fig. 8J, K; for quantification, see Fig. 8L). Thus, the specific increase of *opn*-positive cells in *cyp26b1* mutants (Fig. 8G) might primarily reflect an increase in the activity of osteoblasts (see Discussion).

Inhibition of Cyp26 enzymes during mouse development leads to axial hyperossification and to fusion of cervical vertebrae

To study whether Cyp26 enzymes might have a similar role in restricting ossification during mammalian development, we treated mouse fetuses with the Cyp26 inhibitor R115866, starting at E13, shortly before the onset of vertebral ossification in untreated animals. At E18.5, treated mice often displayed fusions of neural arches of cervical vertebrae, particularly in C3–C5 (Fig. 9A, B) (n=4). However, no fusions were seen in thoracic, sacral or lumbar vertebrae, similar to the cervical restriction of fusions that is seen in several human vertebral disorders. Instead, in posterior regions, treated mice displayed ossification defects within vertebrae, including precocious fusions of neural arches with centra (Fig. 9C, D) (n=9). Also, the ribs were significantly thicker than in untreated embryos. In summary, this indicates that inhibition of Cyp26b1 causes similar shifts in the temporal and spatial pattern of ossification in mammals as in zebrafish.

DISCUSSION

Previous studies have shown that RA signaling plays multiple roles during skeletal patterning and the differentiation of skeletogenic cells. However, genetic evidence for the in vivo role of RA signaling and its inhibition during osteoblast development has thus far been missing. Here, we show that spatiotemporal restriction of RA signaling by Cyp26b1 is required to attenuate osteoblast maturation/activity and ossification during zebrafish and mouse development. These studies reveal a previously unrecognized effect of unrestricted RA signaling on vertebral column formation, which could also be relevant in human congenital disorders with vertebral fusions. Furthermore, we demonstrate an earlier role of Cyp26b1 in skeletal patterning of the neurocranium, consistent with the palatal clefting caused by fetal exposure to teratogenic retinoid doses in human (Lammer et al., 1985; Young et al., 2000).

Cyp26b1-dependent RA restriction is essential for the formation of craniofacial midline cartilages

Zebrafish *cyp26b1* mutants and wild-type embryos treated with RA during the second day of development display very specific deficiencies of cartilaginous elements in the midline of the neurocranium and pharyngeal arches (Fig. 4). Spatial restriction of these defects could be due to functional redundancy between the three Cyp26 paralogs in other craniofacial regions. Consistently, the *cyp26b1* expression domain in the forehead, adjacent to the reported location of precursors of the ethmoid plate, is one of the few *cyp26b1*-specific domains that lack *cyp26a1* and *cyp26c1* expression (Gu et al., 2005) (see Fig. S3A–C in the supplementary material).

What exactly excessive RA is doing to the midline cells remains elusive. In contrast to a recent report (Reijntjes et al., 2007), we found that the migration (see Fig. S5 in the supplementary material) and survival (our unpublished data) of CNC cells was unaffected in *cyp26b1* mutants. In cell culture systems, RA can block chondrocyte specification (Weston et al., 2003). Accordingly, the limb malformations in *Cyp26b1* mutant mice are due to chondrocyte apoptosis, which might result from such failed specification (Yashiro et al., 2004). In *cyp26b1* mutant zebrafish, however, such a mechanism seems unlikely because we could not detect any increase in the number of TUNEL- or Acridine Orange-positive cells in the affected craniofacial domain between 24 and 96 hpf (our unpublished observations). In addition, cell proliferation rates, as determined via anti-phosphohistone H3 immunostaining, appeared unaltered (our unpublished observations). In this light, we currently favor the possibility that Cyp26b1 might interfere with early skeletal patterning; for example, by modulating a morphogenetic effect of an RA gradient to determine differential cell fates, as has recently been reported for Cyp26a1 during hindbrain patterning (White et al., 2007). Indeed, both in the neurocranium and the branchial skeleton, *cyp26b1* is expressed medial to the RA-synthesizing enzyme Aldh1a (see Fig. S3D-G in the supplementary material). This suggests that the craniofacial system might be patterned by a mediolateral RA gradient, with lowest levels in medial positions. This would explain why in *cyp26b1* mutants, only the medial-most cells are lost (Fig. 4J–M). Similarly, the altered neurocranial *col2a1* expression pattern in *cyp26b1* mutants at 50 hpf could indicate that medial positions (normally *col2a1*-negative) have acquired lateral (*col2a1*-positive) fates (Fig. 4C, D).

Cyp26b1-dependent RA restriction is required for proper spatiotemporal control of osteoblast biology and bone formation

In *Cyp26b1* mutant mice, possible defects during bone formation have only been marginally addressed (Yashiro et al., 2004). Also, expression of mouse *Cyp26b1* in osteoblasts has not been described (Abu-Abed et al., 2002). Here, we show that zebrafish *cyp26b1* transcripts

colocalize at least transiently with *osx*, *col10a1* and *opn*, even in developing intramembranous bones that lack chondrocytes, strongly suggesting that *cyp26b1* is expressed in osteoblasts. Our analyses further indicate that *cyp26b1* expression levels are particularly high in immature and/or less active osteoblasts, whereas expression in fully differentiated and/or highly active osteoblasts is much lower, in line with its proposed role in attenuating osteoblast maturation and/or activity. In cell culture systems, RA has also been shown to promote hypertrophic maturation/activity of chondrocytes (Weston et al., 2003). Whether a similar mechanism contributes to the hyperossification of endochondral bones in zebrafish *cyp26b1* mutants remains unclear. However, this seems unlikely because *cyp26b1* is only transiently expressed in chondrocytes and is switched off as they specify (Fig. 2).

In addition to endochondral bones, *cyp26b1* mutants display hyperossification of intramembranous bones, which leads to overgrowth of the elements (Figs 5 and 6). In the vertebral column, this results in a complete fusion of centra (Fig. 6), whereas the opposite phenotype, complete loss of vertebral ossification, is obtained upon *cyp26b1* overexpression (see Fig. S1H in the supplementary material). Vertebral fusions in *cyp26b1* mutants manifest rather late, and cannot be due to shifts in vertebral identities because somitic expression of all tested Hox genes (*hoxc6b*, *hoxc8a*, *hoxb8b*, *hoxb10a*) (Prince et al., 1998) is unaffected at 24 hpf and later (our unpublished observations).

Our in situ hybridization analysis further revealed a precocious initiation of expression and a significant increase in the number of *cyp26b1*- and *opn*-positive cells in *cyp26b1* mutants (Fig. 8; see Fig. S7 in the supplementary material). The precocious expression in ectopic positions could be interpreted as a consequence of premature osteoblast maturation. However, several lines of evidence suggest that in addition to maturation, or even instead of it, RA affects osteoblast activity. First, *cyp26b1* mutants displayed a striking increase in *opn* transcript levels per cell, which, at least in the opercle, clearly preceded the increase in cell numbers. In osteoblast cell cultures, *opn* levels are often used to measure osteoblast activity because they increase in proportion to the amount of mineralized bone material, also in response to RA (Manji et al., 1998; Ohishi et al., 1995; Song et al., 2005). Second, *cyp261* mutants displayed normal numbers of cells expressing other osteoblast markers, *col10a1* and *osx*. This is in striking contrast to the effect of Bmp2 overexpression, a well-studied positive regulator of osteoblast maturation, which caused hyperossification accompanied by an increase of *col10a1*-positive cells (Figs 7 and 8). Finally, axial osteoblasts were still sensitive to RA many days after they had arrived at their final perichordal destination and after they had become insensitive to Bmp2 (15 versus 4 dpf) (compare Fig. 7N with Fig. 3H and Fig. 7P).

In cell culture studies, RA and Bmp2 have also been shown to stimulate osteoclasts, which are bone-resorbing cells of the hematopoietic lineage (Cowan et al., 2005; Kaji et al., 1995). However, for several reasons, this does not seem relevant for the ossification defects of *cyp26b1* mutants. First, we would expect a stimulation of osteoclasts to result in loss, rather than the observed gain, of bone. Second, according to histological stainings of the osteoclast marker enzyme tartrate-resistant acid phosphatase (TRAP; Acp5 – ZFIN), osteoclasts only become active long after the bone phenotype of *cyp26b1* mutants has become apparent (14 dpf) (Gavaia et al., 2006; Witten et al., 2001). Third, knockdown of *pu.1* (Spi1 – ZFIN), which is required for specification of the entire myeloid lineage including osteoclasts (Rhodes et al., 2005; Zhao et al., 2007), did not affect axial ossification, although other myeloid derivatives, such as *mpx*-positive neutrophils, were completely absent (our unpublished results). This suggests that in contrast to Cyp26b1 and osteoblasts, osteoclasts are dispensable for bone formation during the larval stages we have investigated.

Cyp26b1 and human disease: is *dolphin* a model for Klippel-Feil anomaly (KFA) or related syndromes?

In higher vertebrates, such as birds and mammals, vertebra formation occurs via endochondral ossification, whereas in teleosts, vertebral bodies are formed through direct ossification in and around the notochordal sheath (perichordal centra). There has been some debate about the involvement of osteoblasts in fish axial skeleton development. According to one report, vertebral bodies in zebrafish arise by secretion of bone matrix from the notochord and without any involvement of osteoblasts (Fleming et al., 2004). By contrast, a more recent report claims that sclerotome-derived osteoblasts are present in intervertebral regions in Medaka (Inohaya et al., 2007). Our data are consistent with the latter report and with the situation in higher vertebrates, pointing to the presence and activity of osteoblasts during vertebral ossification in zebrafish. In addition, our data indicate that the role of Cyp26 enzymes in preventing hyperossification and vertebrae fusions has been largely conserved between fish and mammals. Mouse *Cyp26b1* displays metameric expression in the developing vertebral column (Abu-Abed et al., 2002), which could correspond to the *cyp26b1* expression in intervertebral regions described here. *Cyp26b1* mouse mutants have been reported to display a fusion of the two first cervical vertebrae, atlas and axis (G. A. MacLean, PhD thesis, Queen's University Kingston, Ontario, Canada, 2007; http://hdl.handle.net/1974/750). It had been proposed that this fusion is due to RA-induced homeotic transformations in vertebral anterior-posterior (AP) identity. However, we show here that inhibition of Cyp26 activity leads to hyperossifications and to fusions of cervical vertebrae when the drug is applied days after vertebral AP identity has been determined (E9–11) (Kessel, 1992; Kessel and Gruss, 1991). This suggests that, as in zebrafish, mouse Cyp26 enzymes are required to regulate ossification.

In humans, several disorders with cervical vertebral fusions have been described. A rather common (1:40,000) congenital disorder with such fusions is Klippel-Feil anomaly (KFA; OMIM 118100) (Kaplan et al., 2005; Tracy et al., 2004). KFA occurs sporadically, as well as in families with dominant or recessive inheritance. Its aetiology is unknown. Vertebral fusion is variably associated with craniofacial abnormalities, including frontonasal dysplasia, and various limb malformations. A similar association of vertebral and other developmental defects is observed in Goldenhar syndrome (OMIM 164210), MURCS association (OMIM 601076) and VATER association (OMIM 192350).

Zebrafish *cyp26b1* mutants display a reduction in the anterior neurocranium and compromised pectoral fin development, consistent with frontonasal and limb abnormalities seen in some of the human syndromes. Homozygous null mutants die during late larval stages (10–15 dpf); however, hypomorphic alleles are sub-viable and characterized by progressive vertebral defects (Spoorendonk et al., 2008). Similar mutations could account for recessively inherited cases of human KFA, whereas the sporadic or dominantly inherited cases could be due to haploinsufficiencies of null mutations, as described here for the zebrafish *ti230g* allele, or to antimorphic mutations.

Interestingly, a sporadic case of KFA associated with craniofacial and ear defects has been correlated with an inversion on chromosome 2(p12q34) (Papagrigorakis et al., 2003). The human *CYP26B1* gene is located at 2p13, close to this breakpoint. In collaboration with human geneticists, we are currently readdressing this case, and are sequencing *CYP26B1* from other subjects with diagnosed KFA or Goldenhar syndrome (McGaughran et al., 2003).

Supplementary Material

Refer to Web version on PubMed Central for supplementary material.

Acknowledgments

We thank Elisabeth Busch and Derek Stemple for providing the *sa0002* allele; Lieven Meerpoel (Johnson and Johnson Pharmaceutical Research and Development) for free samples of R115866; Cecilia Moens, Charles Kimmel, Vicky Prince and Tom Schilling for zebrafish reagents; Caroline Johner and Norbert Joswik for their help with the mouse experiments; Tom Schilling, Shannon Fisher, Henry Roehl and Jochen Holzschuh for helpful discussions; and Kirsten Spoorendonk and Stefan Schulte Merker for sharing unpublished data. Work in the laboratory of M.H. and the TILLING project leading to the isolation of the *sa0002* allele were supported by the European Union (6th Framework Integrated Project 'Zebrafish Models for Human Development and Disease').

References

Abu-Abed S, Dolle P, Metzger D, Beckett B, Chambon P, Petkovich M. The retinoic acid-metabolizing enzyme, CYP26A1, is essential for normal hindbrain patterning, vertebral identity, and development of posterior structures. Genes Dev. 2001; 15:226–240. [PubMed: 11157778]

Abu-Abed S, MacLean G, Fraulob V, Chambon P, Petkovich M, Dolle P. Differential expression of the retinoic acid-metabolizing enzymes CYP26A1 and CYP26B1 during murine organogenesis. Mech Dev. 2002; 110:173–177. [PubMed: 11744378]

Adams SL, Cohen AJ, Lassova L. Integration of signaling pathways regulating chondrocyte differentiation during endochondral bone formation. J Cell Physiol. 2007; 213:635–641. [PubMed: 17886256]

Akimenko MA, Ekker M, Wegner J, Lin W, Westerfield M. Combinatorial expression of three zebrafish genes related to *distal-less*: part of a homeobox gene code for the head. J Neurosci. 1994; 16:3475–3486. [PubMed: 7911517]

Alford AI, Hankenson KD. Matricellular proteins: extracellular modulators of bone development, remodeling, and regeneration. Bone. 2006; 38:749–757. [PubMed: 16412713]

Avaron F, Hoffman L, Guay D, Akimenko MA. Characterization of two new zebrafish members of the Hedgehog family: atypical expression of a zebrafish *indian hedgehog* gene in skeletal elements of both endochondral and dermal origins. Dev Dyn. 2006; 235:478–489. [PubMed: 16292774]

Begemann G, Schilling TF, Rauch GJ, Geisler R, Inghm PW. The zebrafish neckless mutation reveals a requirement for raldh2 in mesodermal signals that pattern the hindbrain. Development. 2001; 128:3081–3094. [PubMed: 11688558]

Begemann G, Marx M, Mebus K, Meyer A, Bastmeyer M. Beyond the neckless phenotype: influence of reduced retinoic acid signaling on motor neuron development in the zebrafish hindbrain. Dev Biol. 2004; 271:119–129. [PubMed: 15196955]

Bird NC, Mabee PM. Developmental morphology of the axial skeleton of the zebrafish, Danio rerio (Ostariophysi: Cyprinidae). Dev Dyn. 2003; 228:337–357. [PubMed: 14579374]

Blomhoff R, Blomhoff HK. Overview of retinoid metabolism and function. J Neurobiol. 2006; 66:606–630. [PubMed: 16688755]

Chocron S, Verhoeven MC, Rentzsch F, Hammerschmidt M, Bakkers J. Zebrafish Bmp4 regulates left-right asymmetry at two distinct developmental time points. Dev Biol. 2007; 305:577–588. [PubMed: 17395172]

Clay H, Ramakrishnan L. Multiplex fluorescent in situ hybridization in zebrafish embryos using tyramide signal amplification. Zebrafish. 2005; 2:105–111. [PubMed: 18248170]

Colnot C. Cellular and molecular interactions regulating skeletogenesis. J Cell Biochem. 2005; 95:688–697. [PubMed: 15880692]

Cowan CM, Aalami OO, Shi YY, Chou YF, Mari C, Thomas R, Quarto N, Nacamuli RP, Contag CH, Wu B, et al. Bone morphogenetic protein 2 and retinoic acid accelerate in vivo bone formation, osteoclast recruitment, and bone turnover. Tissue Eng. 2005; 11:645–658. [PubMed: 15869441]

Cubbage CC, Mabee PM. Developmental morphology of the axial skeleton of the zebrafish, Danio rerio (ostariophysi: Cyprinidae). J Morphol. 1996; 129:121–160.

Du SJ, Frenkel V, Kindschi G, Zohar Y. Visualizing normal and defective bone development in zebrafish embryos using the fluorescent chromophore calcein. Dev Biol. 2001; 238:239–246. [PubMed: 11784007]

Eberhart JK, Swartz ME, Crump JG, Kimmel CB. Early hedgehog signaling from neural to oral epithelium organizes anterior craniofacial development. Development. 2006; 133:1069–1077. [PubMed: 16481351]

Echeverri K, Oates AC. Coordination of symmetric cyclic gene expression during somitogenesis by Suppressor of Hairless involves regulation of retinoic acid catabolism. Dev Biol. 2007; 301:388–403. [PubMed: 17098223]

Elizondo MR, Arduini BL, Paulsen J, MacDonald EL, Sabel JL, Henion PD, Cornell RA, Parichy DM. Defective skeletogenesis with kidney stone formation in dwarf zebrafish mutant for trpm7. Curr Biol. 2005; 15:667–671. [PubMed: 15823540]

Emoto Y, Wada H, Okamoto H, Kudo A, Imai Y. Retinoic acid-metabolizing enzyme Cyp26a1 is essential for determining territories of hindbrain and spinal cord in zebrafish. Dev Biol. 2005; 278:415–427. [PubMed: 15680360]

Fleming A, Keynes R, Tannahill D. A central role for the notochord in vertebral patterning. Development. 2004; 131:873–880. [PubMed: 14736741]

Flores MV, Tsang KWK, Hu W, Kalev-Zylinska M, Postlethwait J, Crosier P, Crosier K, Fisher S. Duplicate zebrafish runx2 orthologues are expressed in developing skeletal elements. Gene Expr Patterns. 2004; 4:573–581. [PubMed: 15261836]

Flores MV, Lam EY, Crosier P, Crosier K. A hierarchy of Runx transcription factors modulate the onset of chondrogenesis in craniofacial endochondral bones in zebrafish. Dev Dyn. 2006; 235:3166–3176. [PubMed: 17013873]

Fujii H, Sato T, Kaneko S, Gotoh O, Fujii-Kuriyama Y, Osawa K, Kato S, Hamada H. Metabolic inactivation of retinoic acid by a novel P450 differentially expressed in developing mouse embryos. EMBO J. 1997; 16:4163–4173. [PubMed: 9250660]

Gavaia PJ, Simes DC, Ortiz-Delgado JB, Viegas CS, Pinto JP, Kelsh RN, Sarasquete MC, Cancela ML. Osteocalcin and matrix Gla protein in zebrafish (Danio rerio) and Senegal sole (Solea senegalensis): comparative gene and protein expression during larval development through adulthood. Gene Expr Patterns. 2006; 6:637–652. [PubMed: 16458082]

Gu X, Xu F, Wang X, Gao X, Zhao Q. Molecular cloning and expression of a novel CYP26 gene (cyp26d1) during zebrafish early development. Gene Expr Patterns. 2005; 5:733–739. [PubMed: 15979416]

Hammerschmidt M, Pelegri F, Mullins MC, Kane DA, van Eeden FJM, Granato M, Brand M, Furutani-Seiki M, Haffter P, Heisenberg CP, et al. *dino* and *mercedes*, two genes regulating dorsal development in the zebrafish embryo. Development. 1996; 123:95–102. [PubMed: 9007232]

Hernandez RE, Putzke AP, Myers JP, Margaretha L, Moens CB. Cyp26 enzymes generate the retinoic acid response pattern necessary for hindbrain development. Development. 2007; 134:177–187. [PubMed: 17164423]

Inohaya K, Takano Y, Kudo A. The teleost intervertebral region acts as a growth center of the centrum: *in vivo* visualization of osteoblasts and their progenitors in transgenic fish. Dev Dyn. 2007; 236:3031–3046. [PubMed: 17907202]

Isogai S, Lawson ND, Torrealday S, Horiguchi M, Weinstein BM. Angiogenic network formation in the developing vertebrate trunk. Development. 2003; 130:5281–5290. [PubMed: 12954720]

Iwamoto M, Golden EB, Adams SL, Noji S, Pacifici M. Responsiveness to retinoic acid changes during chondrocyte maturation. Exp Cell Res. 1993; 205:213–224. [PubMed: 8387013]

Kaji H, Sugimoto T, Kanatani M, Fukase M, Kumegawa M, Chihara K. Retinoic acid induces osteoclast-like cell formation by directly acting on hemopoietic blast cells and stimulates osteopontin mRNA expression in isolated osteoclasts. Life Sci. 1995; 56:1903–1913. [PubMed: 7746099]

Kaplan KM, Spivak JM, Bendo JA. Embryology of the spine and associated congenital abnormalities. Spine J. 2005; 5:564–576. [PubMed: 16153587]

Karsenty G, Wagner EF. Reaching a genetic and molecular understanding of skeletal development. Dev Cell. 2002; 2:389–406. [PubMed: 11970890]

Kawasaki K, Suzuki T, Weiss KM. Genetic basis for the evolution of vertebrate mineralized tissues. Proc Natl Acad Sci USA. 2004; 101:11356–11361. [PubMed: 15272073]

Kessel M. Respecification of vertebral identities by retinoic acid. Development. 1992; 115:487–501. [PubMed: 1358593]

Kessel M, Gruss P. Homeotic transformations of murine vertebrae and concomitant alteration of Hox codes induced by retinoic acid. Cell. 1991; 67:89–104. [PubMed: 1680565]

Kimmel CB, Ullmann B, Walker M, Miller CT, Crump JG. Endothelin 1-mediated regulation of pharyngeal bone development in zebrafish. Development. 2003; 130:1339–1351. [PubMed: 12588850]

Kudoh T, Wilson SW, Dawid IB. Distinct roles for Fgf, Wnt and retinoic acid in posteriorizing the neural ectoderm. Development. 2002; 129:4335–4346. [PubMed: 12183385]

Lammer EJ, Chen DT, Hoar RM, Agnish ND, Benke PJ, Braun JT, Curry CJ, Fernhoff PM, Grix AW Jr, Lott IT, et al. Retinoic acid embryopathy. N Engl J Med. 1985; 313:837–841. [PubMed: 3162101]

Laue K, Daujat S, Crump JG, Plaster N, Roehl HH, Kimmel CB, Schneider R, Hammerschmidt M. The multidomain protein Brpf1 binds histones and is required for Hox gene expression and segmental identity. Development. 2008; 135:1935–1946. [PubMed: 18469222]

MacLean G, Abu-Abed S, Dolle P, Tahayato A, Chambon P, Petkovich M. Cloning of a novel retinoic-acid metabolizing cytochrome P450, Cyp26B1, and comparative expression analysis with Cyp26A1 during early murine development. Mech Dev. 2001; 107:195–201. [PubMed: 11520679]

MacLean G, Li H, Metzger D, Chambon P, Petkovich M. Apoptotic extinction of germ cells in testes of Cyp26b1 knockout mice. Endocrinology. 2007; 148:4560–4567. [PubMed: 17584971]

Manji SS, Ng KW, Martin TJ, Zhou H. Transcriptional and posttranscriptional regulation of osteopontin gene expression in preosteoblasts by retinoic acid. J Cell Physiol. 1998; 176:1–9. [PubMed: 9618139]

Mariani FV, Martin GR. Deciphering skeletal patterning: clues from the limb. Nature. 2003; 423:319–325. [PubMed: 12748649]

McGaughran JM, Oates A, Donnai D, Read AP, Tassabehji M. Mutations in PAX1 may be associated with Klippel-Feil syndrome. Eur J Hum Genet. 2003; 11:468–474. [PubMed: 12774041]

Morin-Kensicki EM, Eisen JS. Sclerotome development and peripheral nervous system segmentation in embryonic zebrafish. Development. 1997; 124:159–167. [PubMed: 9006077]

Nakashima K, Zhou X, Kunkel G, Zhang Z, Deng JM, Behringer RR, de Crombrugghe B. The novel zinc finger-containing transcription factor osterix is required for osteoblast differentiation and bone formation. Cell. 2002; 108:17–29. [PubMed: 11792318]

Nasevicius A, Ekker SC. Effective targeted gene 'knockdown' in zebrafish. Nat Genet. 2000; 26:216–220. [PubMed: 11017081]

Nica G, Herzog W, Sonntag C, Nowak M, Schwarz H, Zapata AG, Hammerschmidt M. Eya1 is required for lineage-specific differentiation, but not for cell survival in the zebrafish adenohypophysis. Dev Biol. 2006; 292:189–204. [PubMed: 16458879]

Niederreither K, Dolle P. Retinoic acid in development: towards an integrated view. Nat Rev Genet. 2008; 9:541–553. [PubMed: 18542081]

Niederreither K, Abu-Abed S, Schuhbaur B, Petkovich M, Chambon P, Dolle P. Genetic evidence that oxidative derivatives of retinoic acid are not involved in retinoid signaling during mouse development. Nat Genet. 2002; 31:84–88. [PubMed: 11953746]

Njar VC, Gediya L, Purushottamachar P, Chopra P, Vasaitis TS, Khandelwal A, Mehta J, Huynh C, Belosay A, Patel J. Retinoic acid metabolism blocking agents (RAMBAs) for treatment of cancer and dermatological diseases. Bioorg Med Chem. 2006; 14:4323–4340. [PubMed: 16530416]

Ohishi K, Nishikawa S, Nagata T, Yamauchi N, Shinohara H, Kido J, Ishida H. Physiological concentrations of retinoic acid suppress the osteoblastic differentiation of fetal rat calvaria cells *in vitro*. Eur J Endocrinol. 1995; 133:335–341. [PubMed: 7581951]

Olsen BR, Reginato AM, Wang W. Bone development. Annu Rev Cell Dev Biol. 2000; 16:191–220. [PubMed: 11031235]

Papagrigorakis MJ, Synodinos PN, Daliouris CP, Metaxotou C. De novo inv(2)(p12q34) associated with Klippel-Feil anomaly and hypodontia. Eur J Pediatr. 2003; 162:594–597. [PubMed: 12827510]

Piotrowski T, Schilling TF, Brand M, Jiang YJ, Heisenberg CP, Beuchle D, Grandel H, van Eeden FJ, Furutani-Seiki M, Granato M, et al. Jaw and branchial arch mutants in zebrafish II: anterior arches and cartilage differentiation. Development. 1996; 123:345–356. [PubMed: 9007254]

Prince VE, Joly L, Ekker M, Ho RK. Zebrafish hox genes: genomic organization and modified colinear expression patterns in the trunk. Development. 1998; 125:407–420. [PubMed: 9425136]

Reijntjes S, Rodaway A, Maden M. The retinoic acid metabolising gene, CYP26B1, patterns the cartilaginous cranial neural crest in zebrafish. Int J Dev Biol. 2007; 51:351–360. [PubMed: 17616924]

Rhodes J, Hagen A, Hsu K, Deng M, Liu TX, Look AT, Kanki JP. Interplay of pu. 1 and gata1 determines myelo-erythroid progenitor cell fate in zebrafish. Dev Cell. 2005; 8:97–108. [PubMed: 15621533]

Schilling TF, Kimmel CB. Musculoskeletal patterning in the pharyngeal segments of the zebrafish embryo. Development. 1997; 124:2945–2960. [PubMed: 9247337]

Shelton DN, Sandoval IT, Eisinger A, Chidester S, Ratnayake A, Ireland CM, Jones DA. Up-regulation of CYP26A1 in adenomatous polyposis coli-deficient vertebrates via a WNT-dependent mechanism: implications for intestinal cell differentiation and colon tumor development. Cancer Res. 2006; 66:7571–7577. [PubMed: 16885356]

Song HM, Nacamuli RP, Xia W, Bari AS, Shi YY, Fang TD, Longaker MT. High-dose retinoic acid modulates rat calvarial osteoblast biology. J Cell Physiol. 2005; 202:255–262. [PubMed: 15389522]

Spoorendonk KM, Peterson-Maduro J, Renn J, Trowe T, Kranenbarg S, Winkler C, Schulte-Merker S. Retinoic acid and Cyp26b1 are critical regulators of osteogenesis in the axial skeleton. Development. 2008; 135:3765–3774. [PubMed: 18927155]

Stemple D. Structure and function of the notochord: an essential organ for chordate development. Development. 2005; 132:2503–2512. [PubMed: 15890825]

Stoppie P, Borgers M, Borghgraef P, Dillen L, Goossens J, Sanz G, Szel H, Van Hove C, Van Nyen G, Nobels G, et al. R115866 inhibits all-trans-retinoic acid metabolism and exerts retinoidal effects in rodents. J Pharmacol Exp Ther. 2000; 293:304–312. [PubMed: 10734183]

Tahayato A, Dolle P, Petkovich M. Cyp26C1 encodes a novel retinoic acid-metabolizing enzyme expressed in the hindbrain, inner ear, first branchial arch and tooth buds during murine development. Gene Expr Patterns. 2003; 3:449–454. [PubMed: 12915310]

Tracy MR, Dormans JP, Kusumi K. Klippel-Feil syndrome: clinical features and current understanding of etiology. Clin Orthop Relat Res. 2004; 424:183–190. [PubMed: 15241163]

Ulsamer A, Ortuno MJ, Ruiz S, Susperregui AR, Osses N, Rosa JL, Ventura F. BMP-2 induces Osterix expression through up-regulation of Dlx5 and its phosphorylation by p38. J Biol Chem. 2008; 283:3816–3826. [PubMed: 18056716]

Wada N, Javidan Y, Nelson S, Carney TJ, Kelsh RN, Schilling TF. Hedgehog signaling is required for cranial neural crest morphogenesis and chondrogenesis at the midline in the zebrafish skull. Development. 2005; 132:3977–3988. [PubMed: 16049113]

Walker MB, Kimmel CB. A two-color acid-free cartilage and bone stain for zebrafish larvae. Biotech Histochem. 2007; 82:23–28. [PubMed: 17510811]

Weston AD, Hoffman LM, Underhill TM. Revisiting the role of retinoid signaling in skeletal development. Birth Defects Res C Embryo Today. 2003; 69:156–173. [PubMed: 12955859]

White JA, Beckett-Jones B, Guo YD, Dilworth FJ, Bonasoro J, Jones G, Petkovich M. cDNA cloning of human retinoic acid-metabolizing enzyme (hP450RAI) identifies a novel family of cytochromes P450. J Biol Chem. 1997; 272:18538–18541. [PubMed: 9228017]

White RJ, Nie Q, Lander AD, Schilling TF. Complex regulation of cyp26a1 creates a robust retinoic acid gradient in the zebrafish embryo. PLoS Biol. 2007; 5:e304. [PubMed: 18031199]

Wienholds E, van Eeden F, Kosters M, Mudde J, Plasterk RH, Cuppen E. Efficient target-selected mutagenesis in zebrafish. Genome Res. 2003; 13:2700–2707. [PubMed: 14613981]

Witten PE, Hansen A, Hall BK. Features of mono- and multinucleated bone resorbing cells of the zebrafish Danio rerio and their contribution to skeletal development, remodeling, and growth. J Morphol. 2001; 250:197–207. [PubMed: 11746460]

Wu X, Shi W, Cao X. Multiplicity of BMP signaling in skeletal development. Ann N Y Acad Sci. 2007; 1116:29–49. [PubMed: 18083919]

Yan YL, Hatta K, Riggleman B, Postlethwait JH. Expression of a type II collagen gene in the zebrafish embryonic axis. Dev Dyn. 1995; 203:363–376. [PubMed: 8589433]

Yashiro K, Zhao X, Uehara M, Yamashita K, Nishijima M, Nishino J, Saijoh Y, Sakai Y, Hamada H. Regulation of retinoic acid distribution is required for proximodistal patterning and outgrowth of the developing mouse limb. Dev Cell. 2004; 6:411–422. [PubMed: 15030763]

Young DL, Schneider RA, Hu D, Helms JA. Genetic and teratogenic approaches to craniofacial development. Crit Rev Oral Biol Med. 2000; 11:304–317. [PubMed: 11021632]

Zhao Q, Dobbs-McAuliffe B, Linney E. Expression of cyp26b1 during zebrafish early development. Gene Expr Patterns. 2005; 5:363–369. [PubMed: 15661642]

Zhao Q, Shao J, Chen W, Li YP. Osteoclast differentiation and gene regulation. Front Biosci. 2007; 12:2519–2529. [PubMed: 17127260]

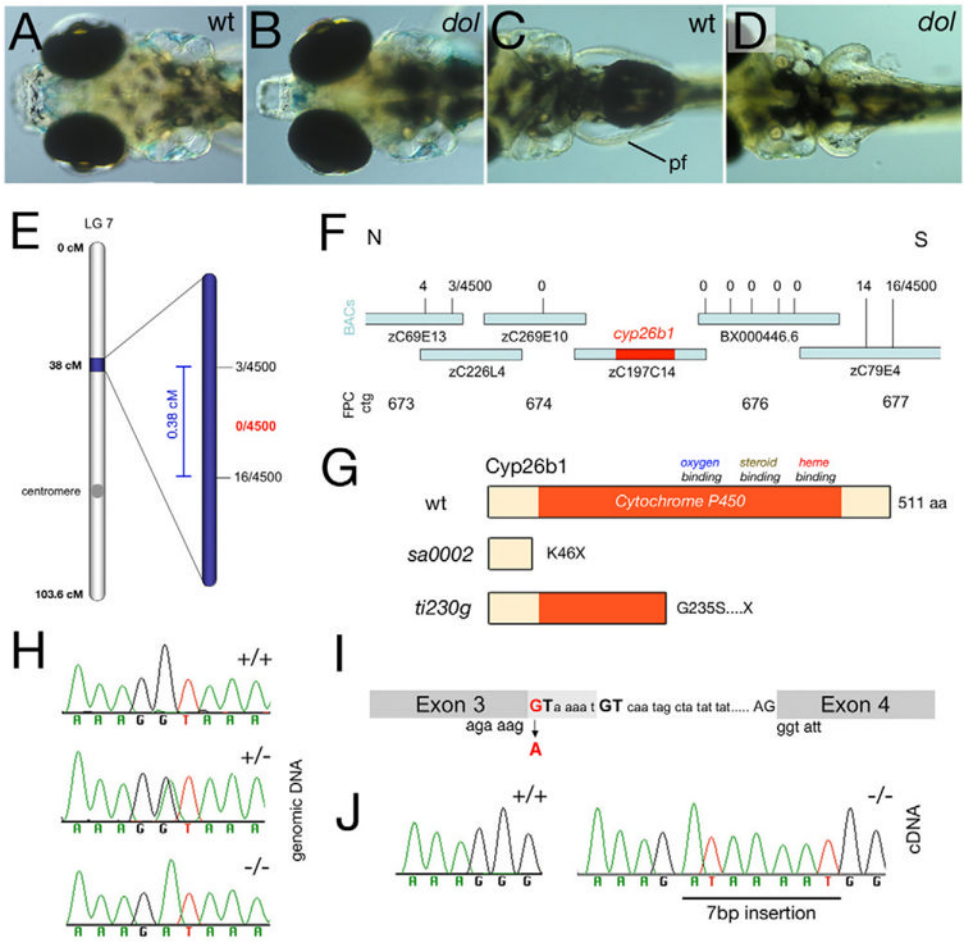

Fig. 1. *dolphin* corresponds to *cyp26b1*

(**A–D**) Live zebrafish larvae at 120 hpf. Dorsal views of head (A, B) and on pectoral fins (pf; C, D). wt, wild type; *dol*, *dolphin* allele *ti230g*. (**E**) The *dol*-bearing interval on chromosome 7. (**F**) Interval-spanning BAC contig, with indicated recombinations in 4500 meioses and showing the location of *cyp26b1* gene. (**G**) Schematic of wild-type and mutant zebrafish Cyp26b1 proteins. (**H**) Sequencing profiles of *cyp26b1* exon 3-intron junction from genomic DNA of wild type (+/+), heterozygous (+/−) and homozygous (−/−) *ti230g* mutants. (**I**) Schematic of exon 3-intron junction of *cyp26b1*. The mutated G in the splice-donor site of the *ti230g* allele is in red, the internal GT used in the mutant is in bold, and the 7 bp insert in mutant cDNA is in light gray. (**J**) Sequencing profiles of *cyp26b1* exon 3-exon 4 junction from cDNA of wild type and *ti230g* mutants. The inserted sequence is underlined.

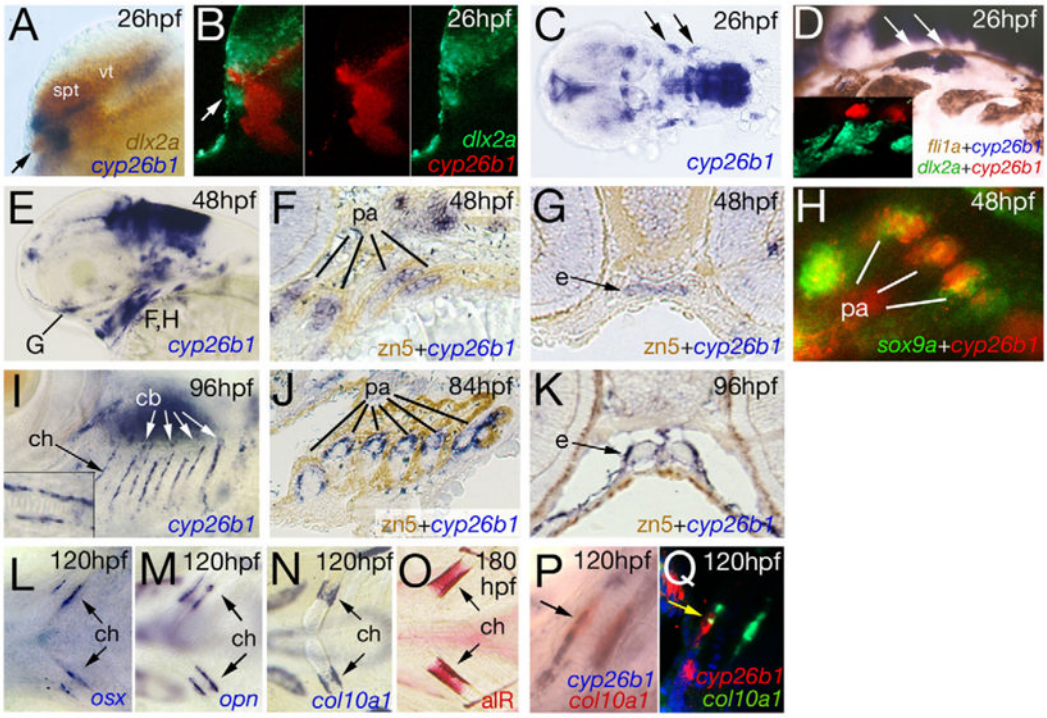

Fig. 2. *cyp26b1* is expressed in condensing chondrocytes and perichondrium

Stainings of wild-type zebrafish at the stages indicated in the upper right corners and with the in situ RNA probes or antibodies indicated in the lower right corners. *fli1a*-positive neural crest cells in D were visualized by anti-GFP immunostaining of a *Tg(fli1a:EGFP)y1* transgenic embryo (Isogai et al., 2003). (A, B, D, E, H, I) Lateral views; (C, L–Q) dorsal views; (F, J) longitudinal sections; (G, K) transverse sections. (**A–D**) *cyp26b1* is expressed close to, but not within, postmigratory cranial neural crest (CNC) cells. Arrows in A, B point to *dlx2a*-positive, *cyp26b1*-negative cells that according to lineage-tracing data are likely to give rise to the ethmoid plate (e). Arrows in C, D point to two *cyp26b1* domains close to the pharyngeal arch-forming CNC. (**E–H**) *cyp26b1* is expressed in chondrogenic mesenchymal condensations. (F, G, H) Magnifications of regions indicated in E. In F, G, pharyngeal endoderm is counterstained with zn5 antibody; in H, neural crest derivatives are stained for *sox9a* transcripts; double-positive domains in pharyngeal arch (pa) condensations are marked. (**I–K**) *cyp26b1* is expressed in perichondrial cells around the pharyngeal arches (J), the ethmoid plate (K), and along the entire length of the ceratohyal (ch) and the ceratobranchials (cb) (I; inset shows magnification of one cb). (**L–Q**) By contrast, *osx* (L), *opn* (M) and *col10a1* (N) are restricted to perichondrial cells around the ossifying, Alizarin Red (alR)-positive region of the ceratohyal (O). In *col10a1*-positive cells, *cyp26b1* levels are lower than in the adjacent *col10a1*-negative perichondrium (P, Q; arrows point to cells double positive for *cyp26b1* and *col10a1*). spt, subpallial telencephalon; vt, ventral thalamus.

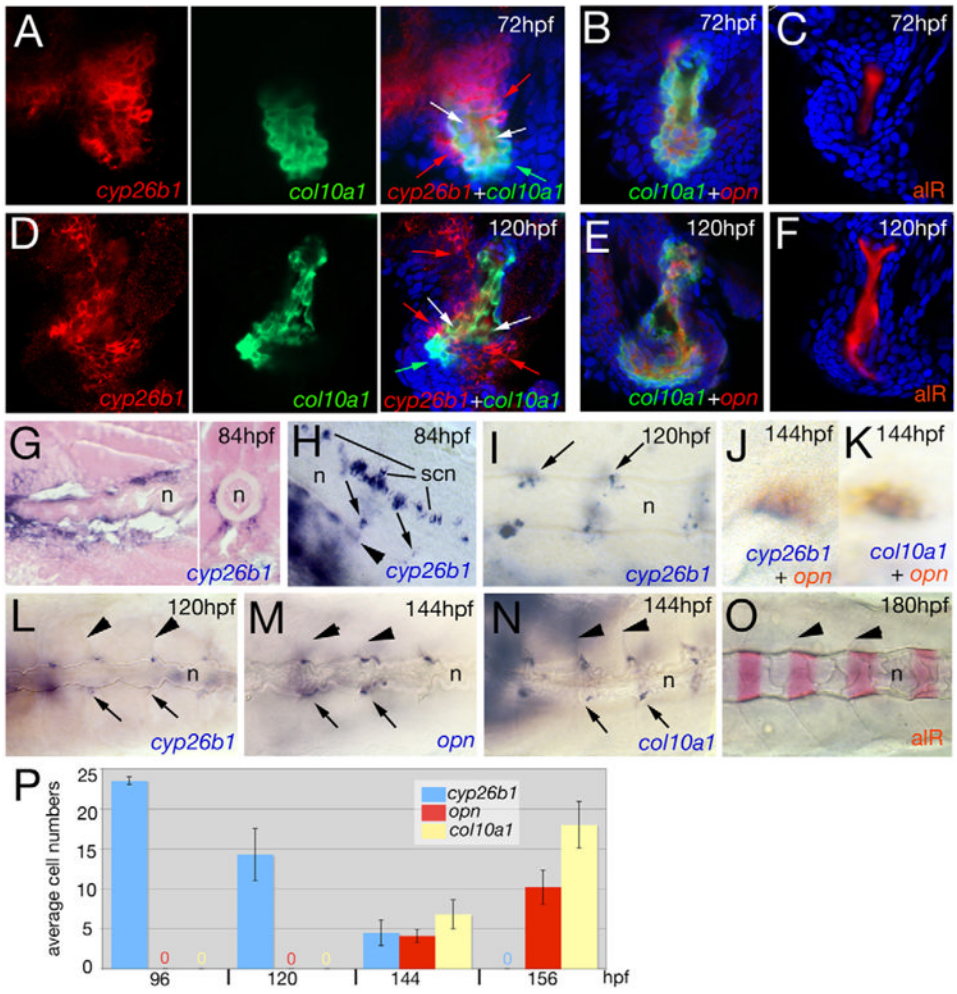

Fig. 3. *cyp26b1* is expressed in osteoblasts and their precursors

Stainings of wild-type zebrafish at the stages indicated in the upper right corners and with the in situ RNA probes indicated in the lower right corners. (**A–F**) Confocal sections of double fluorescent in situ hybridizations and Alizarin Red stainings (alR), counterstained with DAPI (blue). Cells with weak *cyp26b1* and strong *col10a1* expression are indicated with white arrows, cells with strong *cyp26b1* but absent *col10a1* expression with red arrows, and cells with strong *col10a1* but absent *cyp26b1* expression, which most likely represent fully mature/active osteoblasts, with green arrows. See text for details. For single-channel images of B, E, see Fig. S4 in the supplementary material. (**G–I**) *cyp26b1* displays uniform expression in perichordal cells in anterior regions of the notochord (n) (G; left panel shows longitudinal section; right panel shows transverse section; counterstained with Eosin), and metameric expression in the trunk (H, I; lateral views). In H, *cyp26b1*-positive cells are (still) underneath the notochord (arrowhead) and others are (already) in perichordal positions (arrows), whereas in I all cells are perichordal (arrows). Positive cells dorsal of the notochord in H most likely represent ventral spinal cord neurons (scn). (**J–O**) *col10a1* and *opn* show a similar expression pattern to *cyp26b1* (L–N) and transient coexpression with *cyp26b1* (J, K) at intersomitic borders, coincident with the anterior borders of the the Alizarin Red-positive vertebral bodies (O). Arrows in L–N point to positive cells, arrowheads to borders of somites 5–8. (**P**) Numbers of perichordal *cyp26b1*-, *col10a1*- and

opn-positive cells at different developmental time points. Ten fish were evaluated per condition; standard errors are indicated.

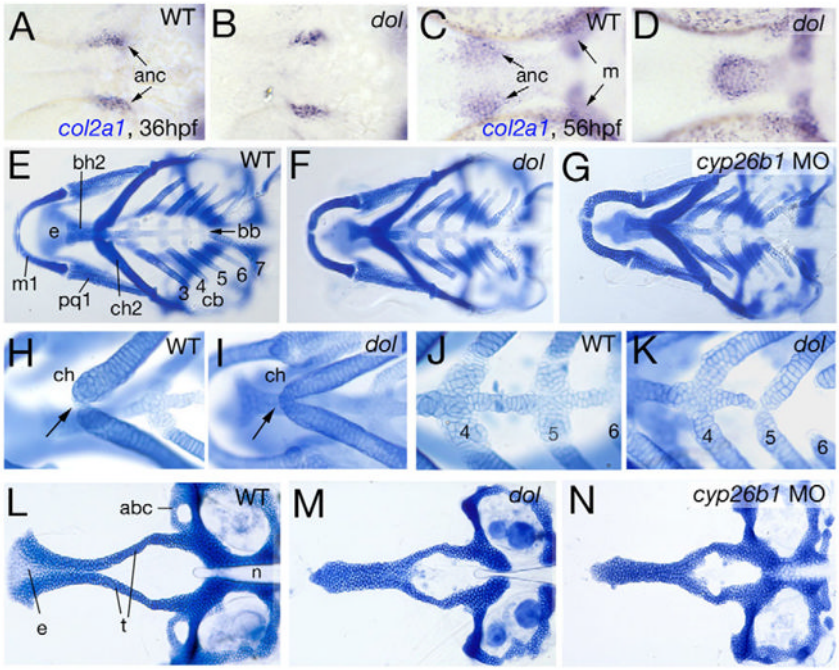

Fig. 4. ***cyp26b1*** **mutants and morphants display deficiencies in midline cartilages of the neurocranium and visceral skeleton**

All panels show ventral views of zebrafish head regions. (**A–D**) *col2a1* in situ hybridization at indicated stages. (**E–N**) Alcian Blue stainings of cartilaginous craniofacial elements at 120 hpf. Pharyngeal arches are numbered (1, mandibulare; 2, hyoid; 3–7, branchial/gill arches 1–5). (E–G) Overviews of visceral skeleton. (H–K) Magnified views of ceratohyals (H, I) or pharyngeal arches 4–6 (J, K). Arrows in H, I point to ceratohyal (ch) attachment in midline. (L–N) Flat-mounts of neurocranium, revealing the absence of medial ethmoid (e) and anterior basicranial commissure (abc) in mutant and morphant. anc, chondrocytes of anterior neurocranium; bb, basibranchial; bh, basihyal; cb, ceratobranchials; m, Meckel's cartilage; n, notochord; pq, palatoquadrate; t, trabeculae cranii.

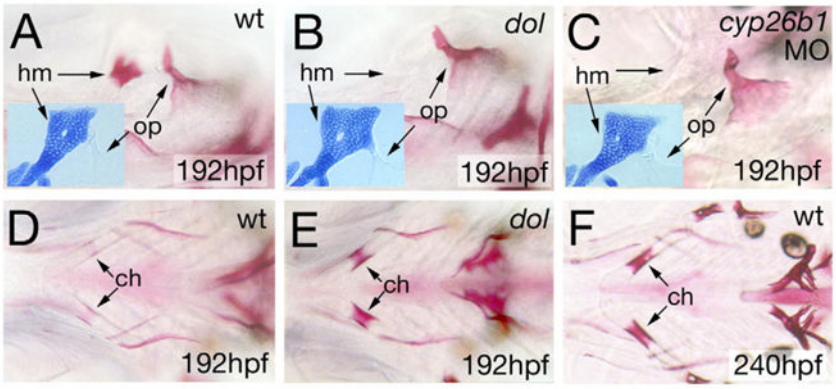

Fig. 5. *cyp26b1* mutants and morphants display increased ossification of endochondral and intramembranous craniofacial bones

(**A–C**) Lateral views and (**D–F**) ventral views of zebrafish larval heads after staining of ossified matrix with Alizarin Red at indicated ages. Insets in A–C show hyomandibula (hm; dorsal element of arch 2) of larvae of same genotype stained with Alcian Blue at 120 hpf. Mutant and morphant show an opercle (op) of increased size, whereas the hyomandibula fails to ossify, although its cartilage model is properly formed (insets). A similar combination of gain of opercle and loss of hyomandibula ossification has previously been described for *endothelin* mutants (Kimmel et al., 2003), possibly reflecting a morphogenetic effect of signaling to pattern ossification along the dorsoventral axis of the second arch and its associated elements. (D–F) Endochondral ossification within the ceratohyal (ch) is much more advanced in the mutant (E), comparable to the situation in a wild-type sibling 2 days later (F).

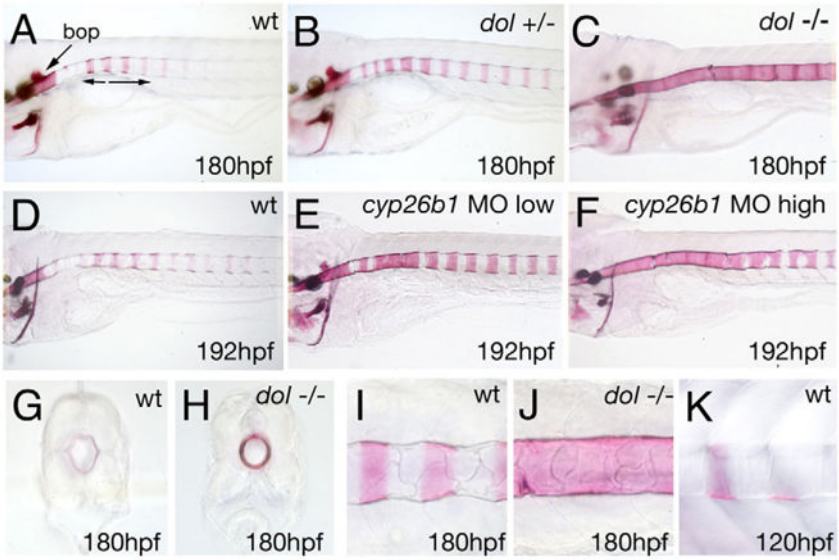

Fig. 6. *cyp26b1* mutants and morphants display precocious and increased ossification of vertebral centra in the developing vertebral column

(**A–K**) Alizarin Red stainings of zebrafish larvae of genotype indicated in the upper right corners and at stages indicated in the lower right corners. (A–F, I–K) Lateral views; (G, H) transverse sections. Arrows in A indicate time course of centra ossification, starting at centra 3/4. In contrast to the segmented ossification of the wild-type larva (A, D, I, K), the *cyp26b1* mutant (C, J) and morphant (F) show uniform and caudally extended perichordal ossification. See text for details. bop, basioccipital articulatory process.

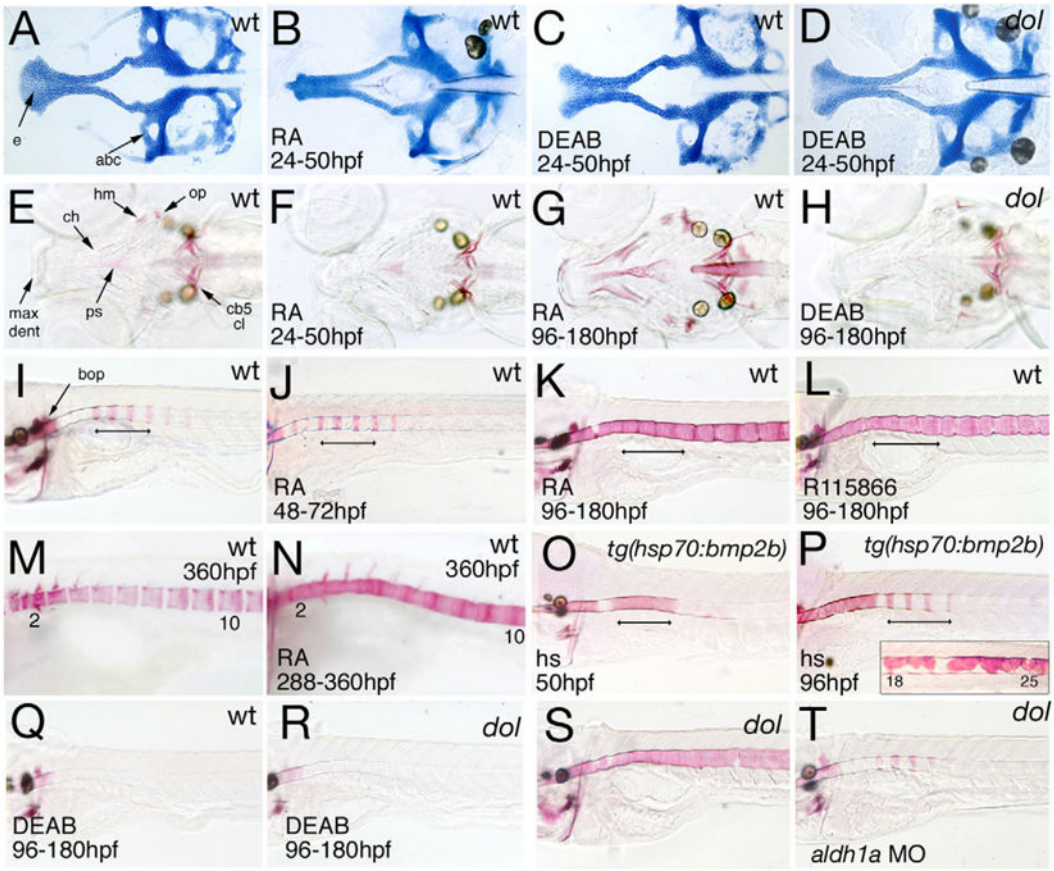

Fig. 7. Retinoic acid (RA) deficiency reverts, whereas RA excess phenocopies, the skeletal alterations of *cyp26b1* mutants, with a pattern of axial hyperossification different from that caused by Bmp2b overexpression

Genotypes are indicated in upper right corners, treatments in lower left corners. (**A–D**) Flat-mounts of Alcian Blue-stained neurocrania after treatment from 24–50 hpf; 120 hpf, dorsal views. Note the absence of the medial ethmoid plate (e) in the RA-treated wild-type zebrafish (B), and the recovery of this structure in the DEAB-treated *cyp26b1* mutant (D). (**E–H**) Alizarin Red-stained heads after treatment from 24–50 hpf (F) or from 96–180 hpf (G, H); 180 hpf, dorsal views. Late (G), but not early (F), RA treatment phenocopies hyperossification of craniofacial bones, whereas late DEAB treatment reverses the mutant phenotype and causes delayed ossification (H). (**I–T**) Alizarin Red-stained centra after treatment with RA (J, K, N), R115866 (L), DEAB (Q, R) or heat shock (hs; O, P) at indicated developmental stages, or after *aldh1a* MO injection (T); 180 hpf(I–L, O–T) or 360 hpf (M, N; vertebrae numbers indicated); lateral views. In I–P, the early-specifiying centra at the level of somites 3–6 are indicated by a bar. Inset in P shows precocious and unsegmented perichordal mineralization at somite levels 18–26 of the same *bmp2b* transgenic animal. See text for details. cb5, ceratobranchial 5 (with teeth); cl, cleithrum; den, dentary; max, maxilla; ps, parasphenoid; see also Figs 4–6.

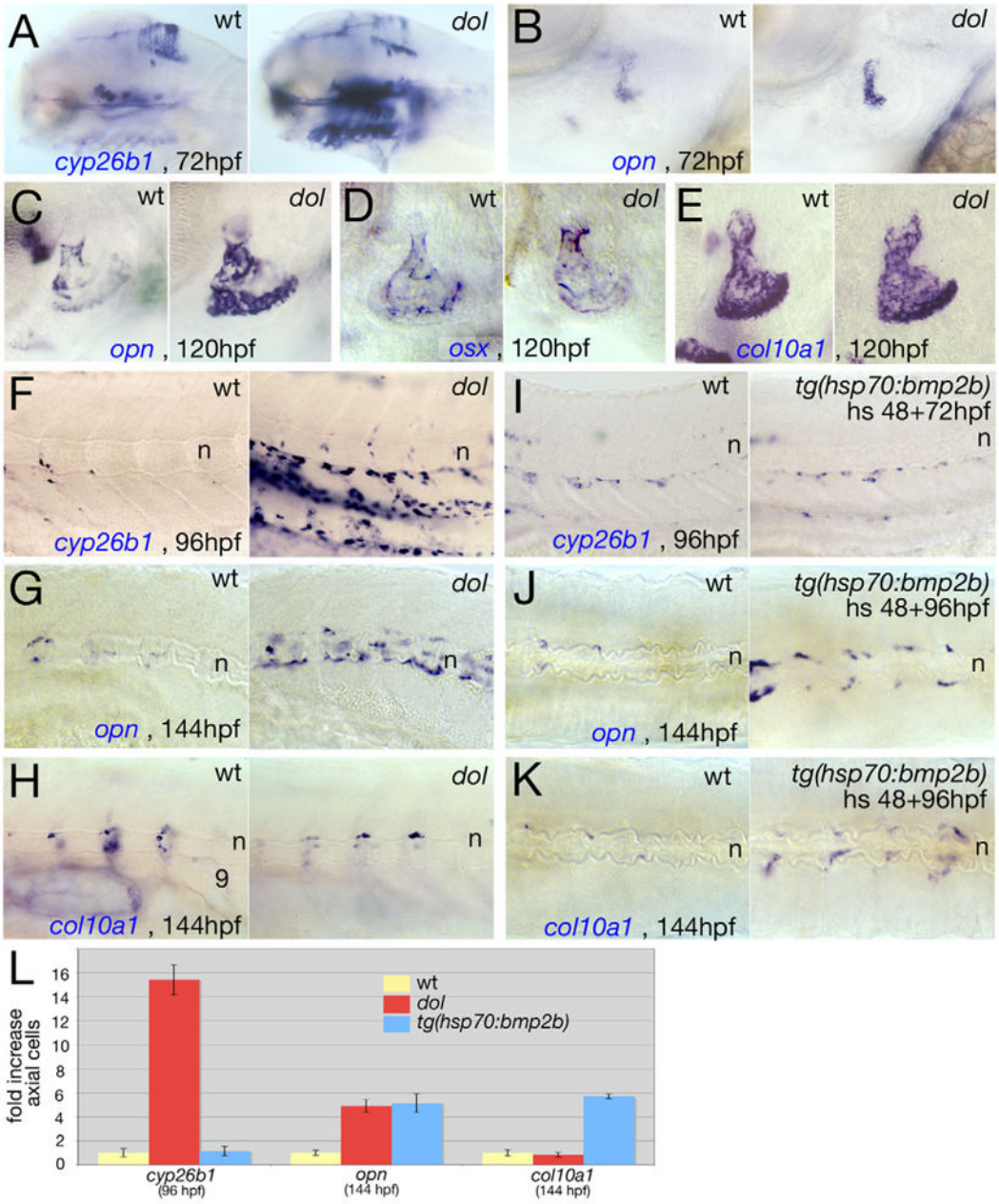

Fig. 8. Loss of *cyp26b1* and gain of Bmp signaling have different effects on the number and/or activity of osteoblasts

(**A–K**) In situ hybridization of zebrafish larvae of genotype indicated in upper right corners and with probes and at stages indicated at lower right corners. (A–I) Lateral views; (J, K) dorsal views. (A) Entire head; (B–E) opercle; (F–K) trunk at level of somites 6–10. In A, stronger c*yp26b1* expression is seen in all craniofacial skeletogenic elements of the *cyp26b1* mutant, but not in the dorsal brain. In G, perichordal *opn*-positive cells of the *cyp26b1* mutant have largely given up their metameric distribution. (**L**) Average increase in the number of axial *cyp26b1*- (at 96 hpf), *opn*- or *col10a1*-positive cells (at 144 hpf) in the trunk/tail region of *cyp26b1* mutants and heat-shocked *Tg(hsp70:bmp2b)* transgenic fish. Control wild-type (wt) siblings were set to a value of 1. Ten fish were counted per condition; standard errors are indicated. n, notochord.

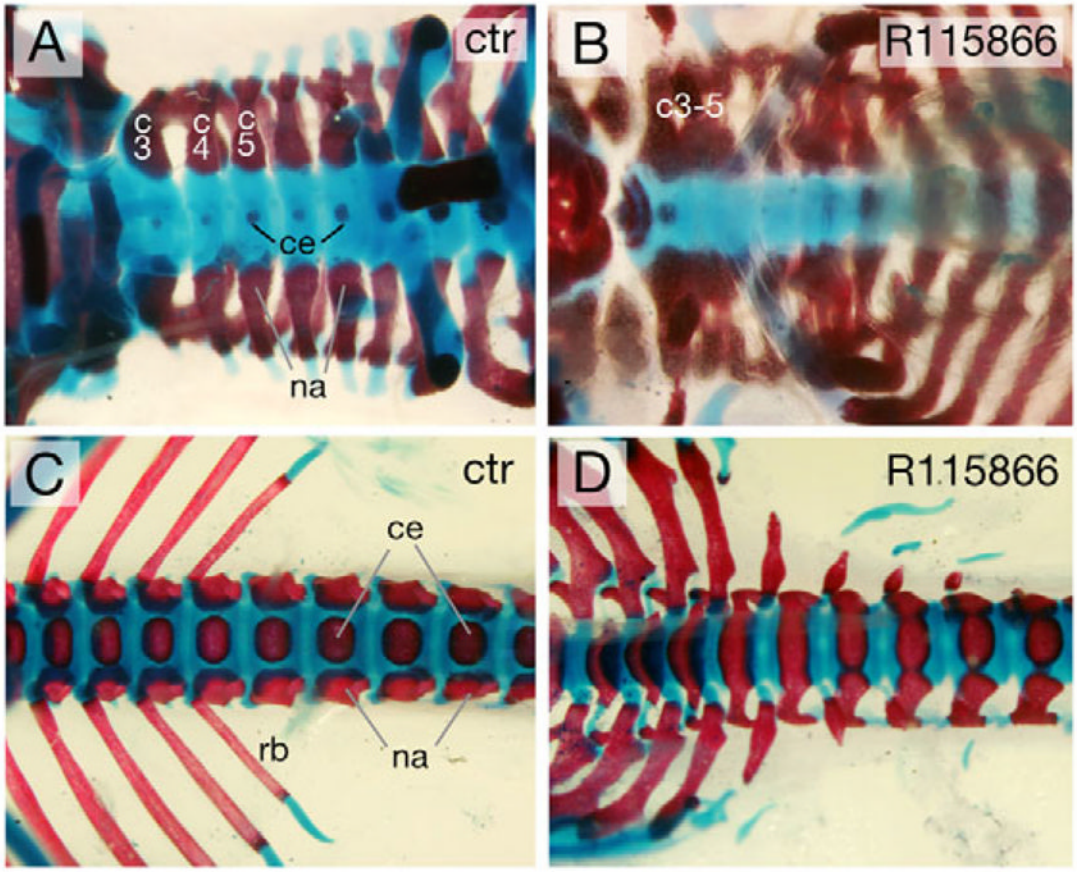

Fig. 9. Treatment of mice with the Cyp26 inhibitor R115866 causes axial hyperossification and fusion of cervical vertebrae

(**A–D**) Alcian Blue (cartilage) and Alizarin Red (bone matrix) stainings of mouse fetuses at E18.5. Dorsal views. (A, C) Control mice treated with vehicle (PEG 200). (B, D) Mice treated with R115866. (A, B) View of cervical vertebrae (c), with fusions of the neural arches of c3– c5 in an R115866-treated animal. (C, D) View of thoracic and sacral vertebrae, with precocious fusions of centra (ce) and neural arches (na), and broader ribs (rb) in the R115866-treated animal.